ACS APPLIED MATERIALS & INTERFACES

Research Article

www.acsami.org

Label-Free Detection of *Staphylococcus aureus* Captured on Immutable Ligand Arrays

Avijit K. Adak,[†] J. William Boley,[‡] David P. Lyvers,[†] George T. Chiu,[‡] Philip S. Low,[†] Ronald Reifenberger,[§] and Alexander Wei*[,†]

[†]Department of Chemistry, [‡]School of Mechanical Engineering, and [§]Department of Physics, Purdue University, West Lafayette, Indiana 47907, United States

Supporting Information

ABSTRACT: The rapid capture and label-free detection of *Staphylococcus aureus*, an opportunistic bacterium that can infect upon contact, can be performed using periodic microarrays of ligand−protein conjugates created by non-contact (inkjet) printing, darkfield imaging conditions, and a FFT-based readout method. Ink solutes were prepared using bovine serum albumin (BSA) conjugated to a glycan with high affinity for bacterial adhesins and printed as dot-matrix arrays with periodicities of 80−120 μm using a thermal injection method. Upon exposing the glycan−BSA microarrays to live strains of *S. aureus*, patterns emerge that can be detected under optical darkfield conditions. These patterns can be decoded by fast Fourier transform (FFT) analysis to generate fault-tolerant readout signals that correspond to the capture of *S. aureus*, with a limit of detection between 10^2 and 10^3 cfu/mL. Inkjet printing provides independent control over array periodicity, enabling FFT signals to be assigned to specific frequencies in reciprocal *k*-space.

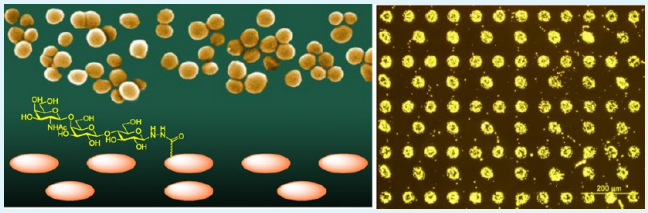

KEYWORDS: *biosensors, Fourier transform, glycans, inkjet printing, microarrays, pathogens*

INTRODUCTION

The rapid detection and identification of bacterial pathogens is of paramount importance for medical diagnostics, transportation biosecurity, and the prevention of global pandemics.[1,2] Outbreaks in public medical facilities and nursing homes are a grave concern; in the US alone, ∼2 million patients per year acquire nosocomial infections, many of them caused by multidrug-resistant strains.[3] The most notorious among these is *Staphylococcus aureus*, an opportunistic Gram-positive bacterium that is often responsible for postoperative infections and is easily transmitted upon contact.[4−6] Bacteremia caused by methicillin-resistant strains of *S. aureus* (MRSA) have become common in hospital settings and are especially difficult to treat, but may be kept under control with adequate surveillance.[7] Several other multidrug-resistant pathogens have also emerged in recent years, creating a strong need to develop platforms capable of multiplex detection of bacteria at or below their infective doses.[8]

Many pathogen detection systems for *S. aureus* and other bacteria are antibody-based.[35−37] However, microbial pathogens are constantly mutating and can therefore produce strains capable of evading detectors that rely on the recognition of nonfunctional surface antigens.[9] We are developing a mutation-resistant alternative to antibody-based detection that exploits the pathogen's native capacity to recognize and bind glycans on the surfaces of host cells[10−12] or specific siderophores used to retrieve essential minerals.[13,16] The recognition of such low-molecular-weight ligands may be deemed "immutable" in the sense that they contribute directly toward pathogen virulence: bacteria that lose their ability to bind such molecules will have also lost their competitive advantage. We have previously vetted this concept using substrates patterned with GalNAc(β1 → 4)Gal(β1 → 4)Glc (**1**),[14] a substructure of ganglioside asialo-GM2 with high affinity for pathogens implicated in respiratory-tract infections,[12] and also with siderophores such as pyoverdine and deferoxamine, which are employed by select pathogens for acquiring iron in mineral-depleted environments.[15,16] Bacteria captured by ligand-patterned substrates can be detected by optical darkfield imaging in 30 min or less, with limits of detection down to 10^2−10^3 cfu/mL. The latter is achieved by a label-free readout method based on Fourier analysis of the bacterial capture patterns, which generates reciprocal lattice peaks that correspond to the periodicity of the immutable ligand array.[17−19]

Fourier analysis also offers a simple but powerful approach toward multiplex pathogen detection using a single chip, based on the emergence of specific capture patterns from multiple, nonoverlapping arrays of immutable ligands. (The latter feature is essential to the reliability of Fourier-based signal generation, as cross-talk created by overlapping array elements can result in false positives.) In the studies above,[14−16] the immutable ligand arrays were produced manually by microcontact printing (μCP) using a polydimethylsiloxane stamp to transfer ligand−BSA conjugates onto gold or functionalized glass substrates.

Received: May 1, 2013
Accepted: June 17, 2013
Published: June 17, 2013

   dx.doi.org/10.1021/am4016236 | *ACS Appl. Mater. Interfaces* 2013, 5, 6404−6411

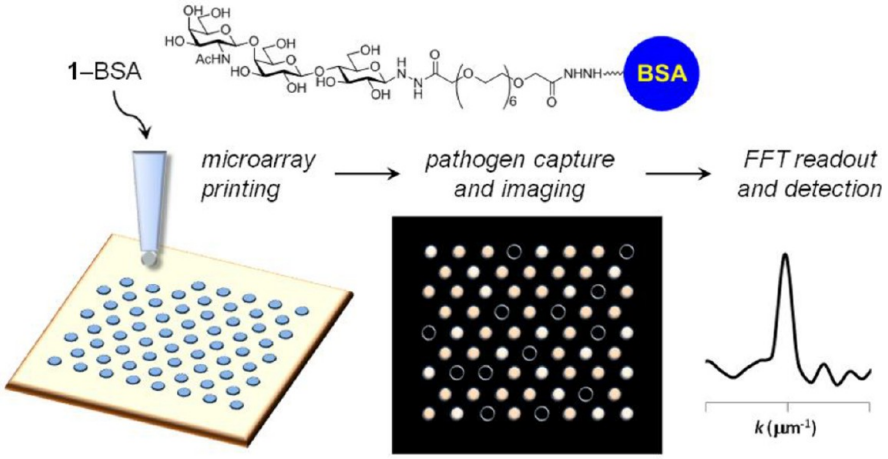

Figure 1. Immutable ligand arrays for bacterial pathogen detection. Left, inkjet deposition of **1**-BSA onto activated glass substrates (with the option of generating multiple periodicities); middle, ligand microarray exposed to pathogens, with label-free imaging of bacteria under darkfield conditions; right, FFT image analysis reveals the emergence of characteristic peaks in Fourier space, corresponding to the periodicity of the capture array.

Although we found μCP to be useful for demonstrating the detection of individual pathogens using our ligand-based arrays, we recognized its limitations for generating nonoverlapping patterns with multiple ligand "inks". Pattern transfer by μCP must be performed one ink at a time, so the registration of multiple microarrays within the same region of interest (ROI) would be challenging in the absence of specialized equipment.

In this work, we evaluate inkjet printing as a practical method for producing nonoverlapping ligand–BSA microarrays for the capture of *S. aureus*, with subsequent detection using a readout algorithm based on fast Fourier transform (FFT) analysis (Figure 1). We present a thermal inkjet method to pattern neoglycoproteins into two interdigitated dot-matrix microarrays with different periodicities and demonstrate their capacity to detect *S. aureus* at concentrations as low as 10^3 cfu/mL. The bacterial capture patterns are imaged by darkfield microscopy and characterized by FFT analysis for quantitative signal readout. The inkjet printer used in this study can deliver drop sizes with a resolution of ~40 μm, but is limited to a single jetting solution. This is, however, sufficient to achieve our objective, which is to show that the interdigitated capture arrays are capable of producing quality signals at specific frequencies in Fourier space and with detection limits well below the threshold of visual inspection. The sensitive detection of *S. aureus* at two independent frequencies also establishes the applicability of this approach toward multiplex pathogen detection.

In the following sections, we first describe the principles behind the FFT-based method of label-free pathogen detection, then validate our approach experimentally with the sensitive detection of *S. aureus* using periodic arrays of glycan **1** conjugated to bovine serum albumin (**1**-BSA). The FFT-based readout produces a quantitative metric for comparing the avidities of various pathogens. It should be emphasized that although affinity microarrays have previously been used to evaluate ligands for pathogen adhesion and binding,[18−21] such arrays have not been developed for pathogen detection by FFT analysis, as described in this article.

EXPERIMENTAL SECTION

Materials. GalNAc(β1 → 4)Gal(β1 → 4)Glc (**1**) was prepared by multistep synthesis as previously described.[14] *N*-Hydroxysuccinimidate (NHS)-activated glass slides (CodeLink and Nexterion H) were purchased from SurModics, Inc. and Schott North America, respectively. Bovine serum albumin (BSA) was purchased in powder form from Sigma and used as received; bacterial culture media (Difco) was obtained from BD Diagnostics. Lyophilized strains of *S. aureus* (ATCC 10537), *Yersinia enterocolitica* (ATCC 51871), and *Pseudomonas aeruginosa* (PA01 strain) were purchased from ATCC. *Vibrio cholerae* (0395) culture was graciously provided by Prof. Shelley Payne (University of Texas, Austin). Deionized water with a resistivity of >18 MΩ·cm^{-1} was obtained from an ultrafiltration system (Milli-Q, Millipore) and passed through a 0.22-μm filter to remove particulate matter.

Neoglycoproteins were prepared using a hexaethyleneglycol–bishydrazide linker as previously described.[14] Freshly prepared solutions of BSA (10 mg) in phosphate buffered solution (PBS, pH 7.4, 200 μL) were treated with 1-ethyl-3-(3-dimethylaminopropyl)-carbodiimide hydrochloride (EDC·HCl, 3 mg in 50 μL of PBS) and gently stirred at room temperature for 1 h. The activated protein solution was then treated for another 2 h with a glycan–bishydrazide conjugate (5 mg) in 200 μL of PBS. The mixture was passed through a 0.45-μm filter to remove aggregates and particulate matter, followed by membrane dialysis (MWCO = 10 kDa). The resulting neoglycoproteins could be stored for several months at 4 °C. Mass spectral analysis of **1**-BSA indicated a median of 5–6 glycans per protein (Figure S1, Supporting Information).

Bacterial Growth Conditions. All microbiological manipulations were performed under biosafety level 2 (BSL-2) conditions, using sterile materials in a microbiological safety cabinet (NU-425-300, Nuaire Inc.). Bacteria strains were grown at 37 °C on a rotary shaker with vigorous agitation in a low CO_2 atmosphere (2.6%), using different growth media: *P. aeruginosa*, *S. aureus*, and *Y. enterocolitica* were cultivated in Difco nutrient broth, and *V. cholerae*, in low-iron T-medium (Tris-buffered minimal medium). The bacteria samples could be centrifuged and stored at −70 °C in glycerol/broth medium (10% v/v) and reactivated by incubating the bacteria in 5 mL of sterile broth medium at 37 °C for 24 h. Bacterial cells were harvested by centrifugation (8050*g* for 5 min) and washed thrice with phosphate buffer (PBS, pH 7.4). The pellets were then resuspended in PBS to a final density of 10^8 cfu/mL (cfu = colony-forming unit). Bacterial counts were established using standard plating methods and correlated with turbidity measurements of culture suspensions. All pathogen detection assays were performed promptly after serial dilution of the bacterial suspensions.

Inkjet Printing. The viscosities of the printing solutions (inks) were characterized by a vibrational viscometer (Viscomate VM-10A). Air–liquid surface tensions were measured using the hanging drop method described by Hansen and Rødsrud;[34] contact angles at the liquid–solid interface were measured by the sessile drop technique.

Measurements were performed with 0.2 wt % solutions of **1**-BSA in PBS containing 0.005% Tween 20, which had a density of 1160 kg/m^3 (±5%), a viscosity of 0.95 mPa-s (±3%), and a surface tension of 49.7 mN/m (±4%) and produced contact angles of 25° and 38° on CodeLink and Nexterion H slides, respectively.

Capture arrays were produced by a stationary HP TIPS thermal droplet ejection system coupled with a motorized *XY* stage (Anorad WKY-150), a laser registration system for mapping the position of the substrate, and an optical imaging camera (Supporting Information Figure S2, S3). The thermal ejection system could be tuned to produce droplet volumes of 1−220 pL, with a displacement uncertainty below 9 μm at 95% confidence. The motorized *XY* stage has an encoder resolution of 0.5 μm with a maximum linear speed of 400 mm/s in each direction and a substrate positioning error of 2−5 μm when subjected to a maximum acceleration of 1.6 m/s^2. The registration system consists of a laser with a beam diameter of 23 μm, reflected into a photodiode connected to a trigger circuit. The imaging system consists of a CCD camera (Sony/XC-ST50, 640 × 480 pixels) with an optical zoom lens for viewing printing results in real time, using a field of view of <5 mm. Visual C-based printing software was written in-house for automated printing protocols using the input bitmap image and pixel resolution to correlate the controller with spot positions. As the stage rasterizes beneath the drop ejector, the controller sends a trigger signal for deposition at prescribed addresses.

A 0.2 wt % solution of **1**-BSA in PBS containing 0.005% Tween 20 was dispensed onto NHS-activated glass slides using the custom-built inkjet printing system described above. A single-channel thermal nozzle with an orifice diameter of 8 μm was positioned ∼0.5 mm above the substrate, with a scan velocity of 1 mm·s^{-1}. An input waveform was applied for droplet generation with a 25-V amplitude and a pulse width of 1.4 μs. Typical print runs produced arrays of 25 × 25 spots with periodicities of 80 or 120 μm in the scanning direction, with an average spot diameter below 50 μm. The glycan−BSA arrays were allowed to sit overnight at 4 °C, then washed sequentially with PBS, PBS containing 0.05% Tween 20, and deionized water. The printed slides were then immersed for 1 h in a buffered solution of ethanolamine (50 mM) using either sodium borate (50 mM, pH 9.2) for Nexterion H slides or Tris-buffered saline (TBS; 100 mM, pH 9.0) for CodeLink slides. The functionalized slides were washed with PBS buffer and deionized water as described above, dried under a stream of nitrogen, then stored at 4 °C until use.

Pathogen Affinity Capture and Image Acquisition. In a typical experiment, glycan capture arrays were incubated with suspensions of live *S. aureus* for 1 h at room temperature and concentrations ranging from 10^7 to 10^2 cfu/mL. The density of live *S. aureus* was estimated by correlating turbidity measurements with colony counts obtained by plating serial dilutions (∼10^8 cfu/mL at O.D. 1, λ = 600 nm). Microarray imaging at each bacterial concentration was performed three times on separate substrates, with each chip supporting two arrays. After incubation, the chip was washed with PBS and deionized water prior to imaging. All darkfield images (before and after exposure to bacteria) were acquired at 10× magnification using an upright microscope (Olympus BH2-RFL-T3) equipped with a darkfield condensor and a DP70 camera (1360 × 1024 pixels). Reflectance images of the captured bacteria were acquired with a resolution of 1 pixel/μm^2, and proved suitable for FFT analysis. We note that pathogen capture patterns were often nonuniform at or near the LOD; nevertheless, their readouts were sufficient for producing signals in Fourier space.

Viability Assay. Immobilized bacteria were stained using a commercial viability kit based on the DNA-staining dyes SYTO 9 and propidium iodide (PI) according to the manufacturer's protocol (LIVE/DEAD BacLight, Invitrogen). In brief, SYTO 9 (1.0 μL, 3.34 mM) and PI (1.0 μL, 20 mM) were combined and diluted with 1 mL of sterile, deionized water. The chip was incubated with the above staining solution for 15 min in the dark, then washed and viewed using a confocal laser-scanning microscope (FV1000, Olympus). The green fluorescence signal of SYTO 9 and red fluorescence signal of PI were detected using excitation/emission wavelengths at 488/500 nm and 520/635 nm, respectively.

FFT Analysis. Darkfield images were cropped and scaled to 512 × 512 pixels (Adobe Photoshop) and saved in TIFF format without compression. Pixels were set in micrometers for ready conversion into reciprocal lattice units (μm^{-1}) in the FFT-derived spectra. 2D-FFT analysis was performed using commercial software (WSxM 4.0 Develop 12.3)[22] with linescans in the *x* direction to evaluate reciprocal lattice peaks characteristic of pathogen capture, as described in the simulations below. The signal quality in the Fourier spectrum was then quantified as the peak signal-to-noise ratio (S/N), which was calculated as the ratio of the peak harmonic intensity to the standard deviation of the residual spectral data between 0 and 0.15 μm^{-1}.

RESULTS AND DISCUSSION

Principles of FFT-Based Pathogen Detection. The Fourier transform decomposes real-space images into their sinusoidal components and maps them into reciprocal (Fourier) space. Each point in the Fourier domain represents the amplitude of a specific wavenumber (one for each dimension) derived from real space. Images with a finite number of array elements are well suited for the discrete Fourier transform (DFT), which is based on a subset of wavenumbers that approximate the main features in real space. For a square image ($L \times L$ μm^2) containing $N \times N$ pixels, the DFT can be expressed as a complex function, $F(k_x, k_y)$:

$$F(k_x, k_y) = \frac{1}{N^2} \sum_{I=0}^{N} \sum_{J=0}^{N} A_{I,J} e^{-2\pi i[k_x I + k_y J]}$$

where A_{IJ} represents the pixel intensity at position (I, J) in real space between $(0, 0)$ and (L, L) and the exponential term specifies the basis function. The value of $F(k_x, k_y)$ provides the amplitude and phase for a given pair of wavenumbers k_x and k_y; the complete set of $F(k_x, k_y)$ values provides a global representation in Fourier space of any relevant periodicities embedded within the original image.

DFT is most efficiently performed by specifying the number of pixels $N = 2^m$, where m is a positive integer. This simple condition allows 2D images to be processed using the FFT algorithm, which reduces the number of necessary operations from N^2 to $N(\log N)$ and produces k_x and k_y values in the range of $\pm(N-1)/L$. In our studies, m is typically 8 or 9 and L is defined in micrometers, so k is presented in units of μm^{-1}. We note that the FFT algorithm can be applied to any digitized image simply by padding it with empty values until an $N \times N$ pixel set is achieved, with m equal to a whole number.

With respect to pathogen detection, the wavenumber k_x matching the fundamental harmonic ($k_1 = \pm 1/a$, where a is the center-to-center distance between array elements) is highly sensitive to the emergence of the periodic pattern formed within the capture array. In this work, we focus only on k_x for analysis, although the microarrays are periodic in both dimensions. In the simulation below, the FFT readout of a dot-matrix array with a spot size of 40 μm (d_{spot}) and a period of 120 μm along the *x* direction (a) produces a peak at k_x = ±0.0083 μm^{-1}, corresponding to k_1 (Figure 2). Smaller contributions are also observed for k_x = ±0.0167 and ±0.025 μm^{-1} ($\pm 2/a$ and $\pm 3/a$, respectively), corresponding to higher-order harmonics k_2 and k_3. However, we find the fundamental harmonic k_1 to be the most practical and reliable signature of pattern recognition because the higher-order harmonics can be influenced by several other structural parameters in addition to the pattern intensity.

The application of FFT-based pattern recognition toward pathogen detection is straightforward and bestows some

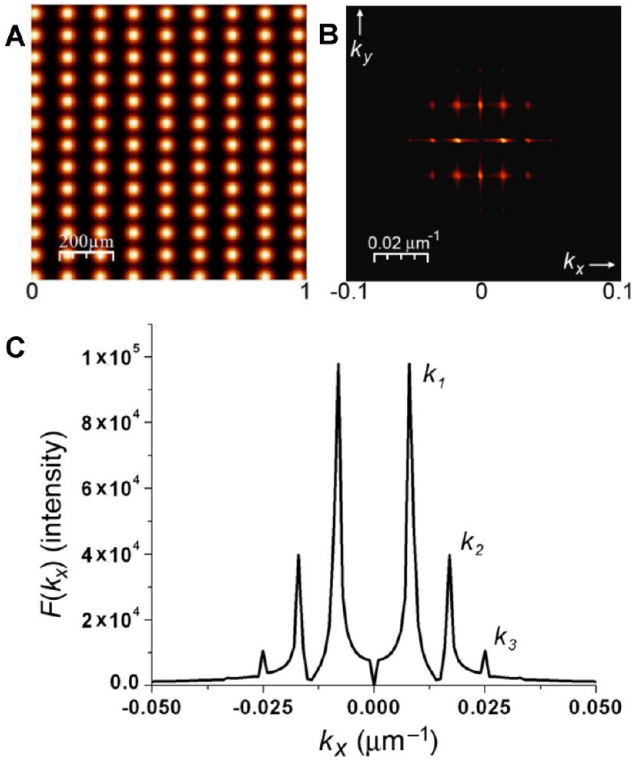

Figure 2. (A) Simulation of a dot-matrix array (a = 120 μm along x, d_{spot} = 40 μm, L = 1 μm); (B) corresponding FFT image (centered at the origin); (C) 1D plot of FFT readout based on linescan along the k_x direction (k_y = 0), with fundamental and higher-order harmonics at k_n = $\pm n/120$ μm^{-1}.

important advantages over other readout methods. One is the ability to detect the emergence of nonzero amplitudes at unique (k_x, k_y) values that are predefined by specific capture patterns, creating opportunities for multiplex detection within the ROI. This is illustrated by simulating pathogen adhesion on two interdigitated capture arrays with different periodicities along the x direction (a = 120 μm; b = 80 μm; Figure 3). FFT analysis of the interdigitated arrays produces a function $F(k_x, k_y)$ that is essentially the sum of the FFT outputs from individual arrays. A plot of the Fourier intensities along k_x (k_y = 0) unambiguously resolves each contribution, with peak k_1 values at $1/a$ and $1/b$ (0.0083 and 0.0125 μm^{-1}, respectively; Figure 3E).

The multiplexing capacity of interdigitated arrays supporting a unique set of k_1 values is ultimately limited by the 2D resolution of the peak signals in the FFT readout, which are influenced by structural factors such as aspect ratio (period-to-spot size, or a/d_{spot}) or the number of array elements within the ROI (Figure 3F). These factors are readily addressed by expanding the size of the ROI and refining the array structure. It is also necessary to avoid overlap between the k_1 peak signals and higher-order harmonics. For example, if periodicities are constrained along one dimension, then the range of possible k_1 values will be bounded by the fundamental and second harmonic of the array with the largest period (a_{max}) such that $1/a_{max} < k_1 < 2/a_{max}$. However, this restriction is artificial to FFT analysis and can be circumvented by designing array patterns that spread the wavenumber-selected peaks across 2D Fourier space.

Additional benefits afforded by the FFT readout are its low instrumentation requirements (darkfield imaging using an objective of medium resolving power, recorded with a CCD camera) and its capacity to detect pathogens at low binding densities with a high level of fault tolerance (Figure 4).[13,14] The emergence of a signature peak at a predefined set of (k_x, k_y) values represents a global average of affinity capture, which is

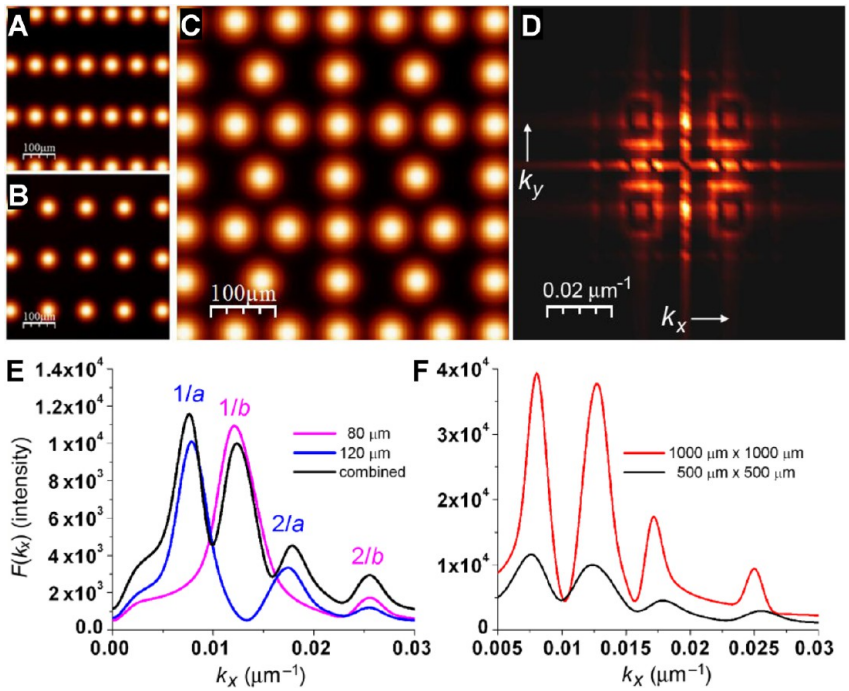

Figure 3. (A–C) Simulation of individual and interdigitated arrays with two different periods (a = 120 μm, b = 80 μm, d_{spot} = 40 μm, L = 500 μm); (D) corresponding FFT analysis of interdigitated arrays; (E) 1D plot of FFT readouts along the k_x direction for images A–C, illustrating their additive nature; (F) FFT signal quality as a function of array size (L = 500 vs 1000 μm), illustrating its impact on peak resolution.

dx.doi.org/10.1021/am4016236 | ACS Appl. Mater. Interfaces 2013, 5, 6404–6411

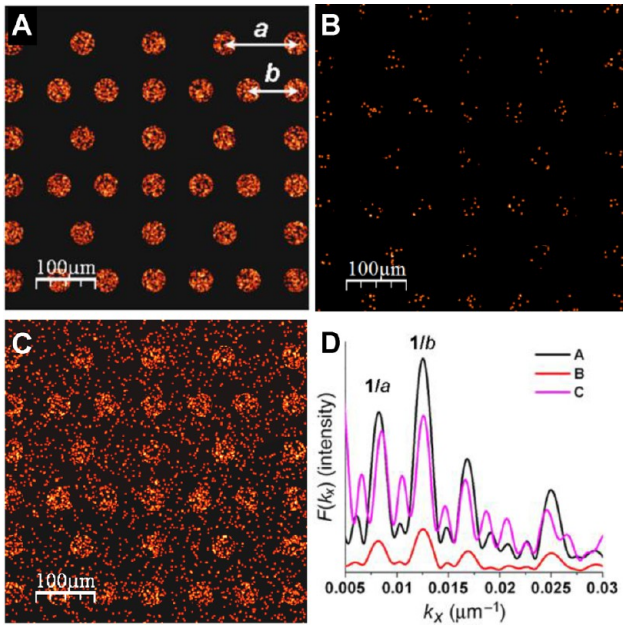

Figure 4. (A, B) Simulations of interdigitated arrays (a = 120 μm, b = 80 μm, d_{spot} = 40 μm) with randomized occupancy factors of 43% and 1%, respectively; image area =500 × 500 μm^2. (C) Simulation of interdigitated array with a similar occupancy factor as in panel A, but with an added background fill factor of 15% to simulate nonspecific binding. (D) 1D plot of FFT readouts along the k_x direction for images A–C, describing signal quality under suboptimal conditions.

more dependable than single-point detection strategies for reporting pathogens at trace levels and also reduces the likelihood of false positives. The requirements for producing signature peaks by FFT analysis are quite robust: wavenumber-selected peaks can be resolved from matrices with low occupancy factors (Figure 4B) or with significant background levels due to nonspecific (random) adsorption (Figure 4C).

Optimization of Inkjet Printing for Pathogen Capture. Various substrate patterning methods can be used to present immutable ligands as periodic arrays, such as photolithography and microcontact printing (μCP);[13,14,23] however, these methods can be troublesome to reproduce and can leave optically detectable marks or residues that are not easily removed by standard washing procedures. For example, we encountered a 10% fail rate in the production of microarrays by μCP. Noncontact methods such as inkjet printing offer greater flexibility and control over the choice of printing parameters and are amenable toward the production of affinity capture chips on a larger scale. Inkjet technologies can dispense droplets of controlled volumes between 1 pL and 5 nL and produce spots as small as 15 μm at precisely defined positions.[24] They are also versatile with respect to formulation: examples of solutes deposited by inkjet include inorganic particles,[25] polymers,[26,27] DNA,[28] and various proteins.[21,29−31]

A 0.2 wt % solution of **1**-BSA in PBS containing nonionic surfactant (0.005 wt % Tween 20) was delivered by thermal droplet ejection onto NHS-activated glass slides (CodeLink or Nexterion H), followed by an incubation period at 4 °C prior to blocking. Droplets on Nexterion H slides formed higher contact angles than those on CodeLink, resulting in less spreading and smaller spot sizes (40 ± 2.1 μm vs 50 ± 2.6 μm), as indicated from the patterns formed by the capture of *S. aureus* (Figure 5A, B). Nexterion H slides were used in all subsequent experiments. We also found 0.005 wt % Tween 20 to be helpful in maintaining cohesion of the picoliter droplets during thermal ejection and in providing uniform coverage within each spot. The latter is attributed to a lower rate of evaporation after deposition: droplets produced without Tween-20 produced ring-like spots upon drying, compromising the uniformity of the periodic array (Figure 5C); however, inks with 0.01 wt % Tween 20 yielded larger spot sizes (Supporting Information Figure S4).

Characterization of Pathogen Capture and Limits of Detection. In our initial studies, arrays of **1**-BSA were exposed for 1 h to suspensions of *S. aureus* at 10^7 cfu/mL, followed by careful rinsing and examination by darkfield microscopy. This imaging method produced high quality signals from the capture arrays and also indicated low levels of nonspecific adsorption (Figure 5A–C). Control experiments established that *S. aureus* binding affinity is specific for glycan **1**: no capture was observed by arrays printed with either unmodified BSA or lactose-

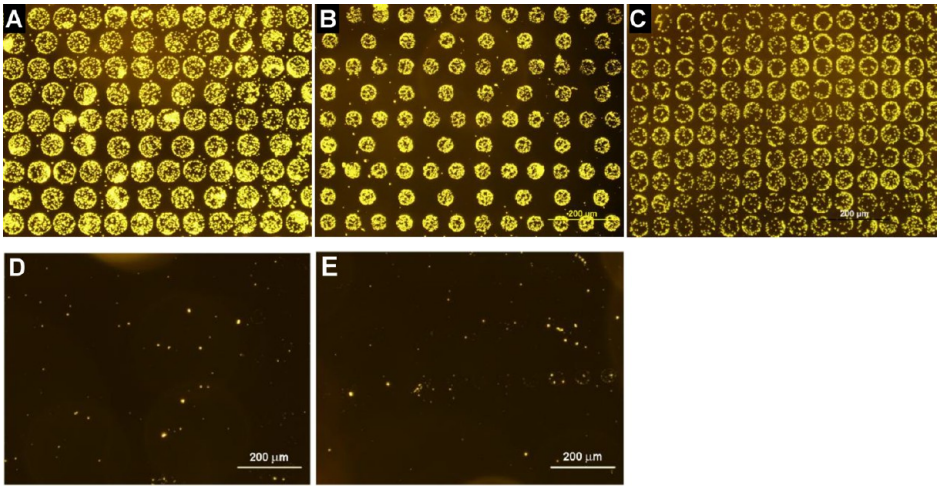

Figure 5. Pathogen capture onto microarrays of **1**-BSA, prepared by thermal inkjet printing. (A,B) *S. aureus* (10^7 cfu/mL) captured by **1**-BSA microarrays printed on functionalized glass slides (CodeLink and Nexterion H, respectively), with 0.005 wt % Tween 20 in the print buffer. (C) *S. aureus* captured onto glass slides patterned with **1**-BSA array, printed without Tween 20. (D, E) Control slides printed with arrays of BSA and lactose-BSA, respectively, after a 1-h exposure to *S. aureus* (10^7 cfu/mL). Scale bar = 200 μm.

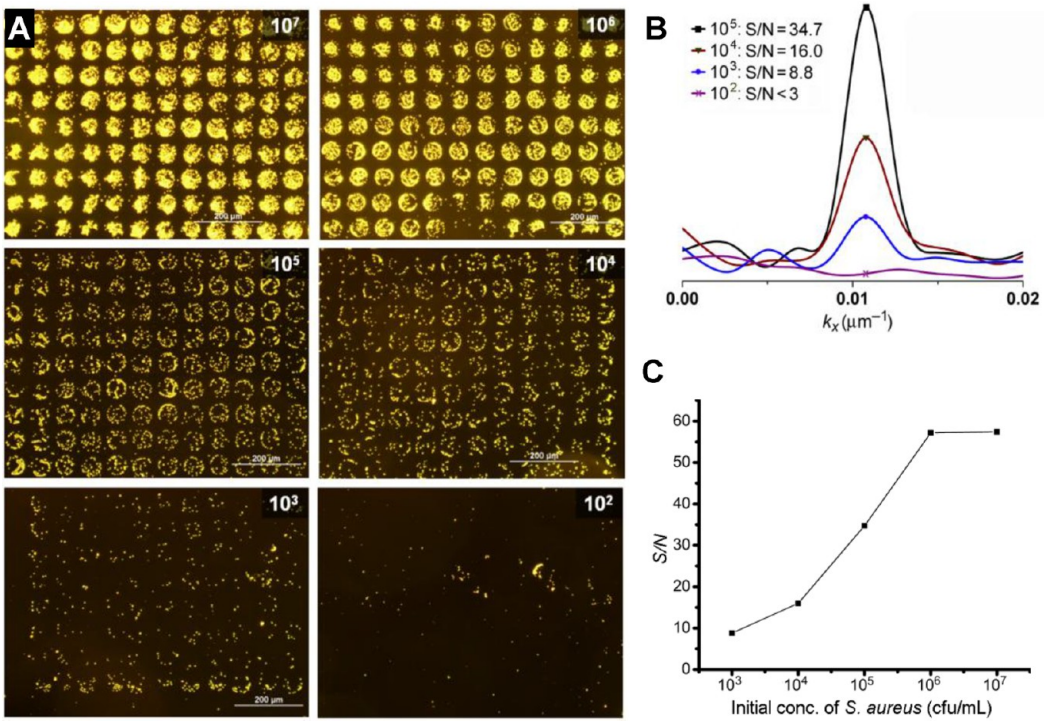

Figure 6. Limit of detection (LOD) for *S. aureus* using **1**-BSA capture arrays. (A) Panel of darkfield images after 1-h exposure to *S. aureus* as a function of concentration, from 10^7 to 10^2 cfu/mL. (B) Fundamental harmonic peaks ($k_1 = 1/80\ \mu m^{-1}$) produced after FFT analysis of capture array images, with S/N values at different pathogen concentrations (cfu/mL). (C) A quasi-linear correlation is observed between initial *S. aureus* concentration and S/N from FFT readout, from 10^3 to 10^6 cfu/mL.

modified BSA (Figure 5D, E). The latter confirms the importance of the terminal 1,4-β-linked GalNAc residue in bacterial recognition, as previously established for *S. aureus* and other pathogens.[14,15,32,33]

Immobilized *S. aureus* were also treated with a DNA staining kit immediately after capture using SYTO-9 (a green fluorescent dye that can permeate intact cell membranes) for total cell imaging and PI (a red fluorescent dye that penetrates cells with damaged membranes) to determine the presence of dead bacteria. The immobilized *S. aureus* were strongly stained by SYTO-9 but only weakly stained by PI, indicating most if not all bacteria were viable at the time of capture (Supporting Information Figure S5). Capture arrays were also exposed to *S. aureus* suspensions (10^7 cfu/mL) previously irradiated for 4 h under UV light (λ_{max} = 254 nm), a condition used for sterilization. No bacteria were captured following a 1-h incubation, and subsequent treatment with SYTO-9/PI yielded no DNA staining (data not shown). This confirmed that the glycan–BSA arrays selectively capture live *S. aureus*, thus permitting detection limits to be defined in terms of colony-forming units.

The limit of detection (LOD) for bacterial pathogens in solution was evaluated by exposing capture arrays of **1**-BSA to suspensions of *S. aureus* for 1 h from 10^7 to 10^2 cfu/mL. Visual inspection of darkfield images revealed well-defined arrays of immobilized *S. aureus* at concentrations above 10^5 cfu/mL, but a significant loss of array definition at concentrations below this level (Figure 6A). Subjecting these optical images to FFT analysis enabled us to confirm the emergence of bacterial patterns using reciprocal lattice peaks at $k = 1/a$ (Figure 6B), and to establish LOD by evaluating peak signal-to-noise ratios in the Fourier spectra (S/N $\geq$ 3). In this study, the LOD of *S. aureus* by the **1**-BSA capture array was determined to be between 10^2 and 10^3 cfu/mL. The sensitivity of the FFT-based readout method is over 2 orders of magnitude higher than other methods that rely on antibody-based detection of *S. aureus*.[36,37]

It is worth noting that (i) the LOD is based on FFT analyses of raw image data, precluding the need for background subtractions, and (ii) a quasilinear correlation can be observed between the S/N and initial pathogen concentration, with signal saturation at 10^6 cfu/mL (Figure 6C). Direct image analysis is possible because the FFT readout is highly fault-tolerant, a major advantage over single-point detection systems. However, background signals can still impact detection limits and Fourier peak intensities due to a trade-off between array occupancy (signal strength) and background noise. When nonspecific binding is low (similar to this work and earlier studies using periodic gratings[14−16]), Fourier peaks can be observed with array occupancy factors as low as 1% (Figure 4B, D), which translates to a LOD in the range of 10^2–10^3 cfu/mL. When the background noise is higher, Fourier peak detection is still readily achieved, but the LOD threshold is raised because of increased spectral noise (Figure 4C, D).

Relative Avidities in Pathogen Binding. GalNAc(β1 → 4)Galβ has been reported to be bound strongly by a number of bacterial pathogens in addition to *S. aureus*, such as *P. aeruginosa* and *Y. enterocolitica*.[12,32] *P. aeruginosa* is a common scourge in hospitals and a major source of respiratory tract infections,[15] whereas *Y. enterocolitica* is well-known for causing enteric diseases.[8] To determine whether these strains demonstrated comparable avidities for trisaccharide **1** under controlled conditions, we used periodic arrays of **1**-BSA to determine the LOD for each of these bacteria and also for *V. cholerae*, which has no reported affinity for **1** (Table 1). The neoglycoprotein arrays were exposed for 1 h to target bacteria

dx.doi.org/10.1021/am4016236 | ACS Appl. Mater. Interfaces 2013, 5, 6404−6411

Table 1. Limits of Detection (LOD) for Bacterial Adhesion onto Capture Arrays of 1-BSA

pathogen	LOD[a] (cfu/mL)
S. aureus	10^3
P. aeruginosa	10^3
Y. enterocolitica	10^6
V. cholerae	*n/a*

[a]Estimated to the nearest order of magnitude, based on the peak quality at $k_1 = 1/a$ in the Fourier spectrum (S/N > 3).

at concentrations up to 10^6 cfu/mL, then washed, imaged, and subjected to FFT analysis as previously described. As expected, *P. aeruginosa* exhibited a high affinity to **1**-BSA with a conservative LOD at 10^3 cfu/mL, similar to an earlier study involving linear gratings prepared by microcontact printing.[14] On the other hand, *Y. enterocolitica* had a low affinity for **1**-BSA, with a LOD of 10^6 cfu/mL, and no capture was observed with *V. cholerae*. Although it has been reported that certain strains of *Yersinia* have an affinity for glycan substructures present in asialo-GM1 and lactosylceramide,[32,38] our results clearly indicate that the affinity of *Y. enterocolitica* to **1**-BSA is orders of magnitude lower than that of *S. aureus* and *P. aeruginosa*, in accord with their respective roles in gastrointestinal and respiratory infections.

FFT Analysis of Pathogen Capture with Binary Arrays. Inkjet printing is ideally suited for creating ligand arrays with different lattice spacings to support multiplex pathogen capture and detection, as suggested in the simulations discussed earlier (Figure 3). To validate this notion experimentally, we prepared interdigitated arrays with two different periodicities using **1**-BSA (a = 120 μm; b = 80 μm), followed by affinity capture of *P. aeruginosa* and FFT analysis to produce the corresponding peaks in reciprocal space. Binary arrays of **1**-BSA were printed in alternating rows along the x direction, programmed according to a 2D input file with a resolution of 20 μm/pixel (Figure 7A). After washing and blocking the substrate as described above, the interdigitated capture arrays were exposed for 1 h to *P. aeruginosa* at a concentration of 10^6 cfu/mL. Darkfield microscopy indicated an efficient capture with homogeneous spot coverage for both arrays (Figure 7B), and FFT analysis and readout revealed two distinct peaks at 1/120 and 1/80 μm^{-1} (Figure 7C), in accord with our earlier simulations. The fundamental harmonic of the smaller array at 1/80 μm^{-1} ($k_1 = 1/b$) is flanked by the second-order harmonic of the larger array at 1/60 μm^{-1} ($k_2 = 2/a$), which serves as a boundary value for additional reciprocal lattice peaks along the k_x direction.

The quality of the analysis in Figure 7 represents an important milestone in establishing the feasibility of the FFT-based approach toward multiplex pathogen detection. The signal intensities of the Fourier peaks at $1/a$ and $1/b$ are comparable, despite the fact that the sizes of the two arrays differ by 50%. In addition, the simulations in Figure 4 illustrate the signal quality of both Fourier peaks at low array occupancy and in the presence of significant noise. These results effectively establish the modest requirements for generating Fourier signals, which can be easily strengthened by increasing the size of the ROI or changing structural factors within the arrays. Although the interdigitated arrays in the present study were printed using a single capture ligand, a multichannel printer would enable the fabrication of capture arrays with orthogonal recognition ligands, each encoded by a unique period to enable the multiplex detection of specific pathogens. This objective is now being pursued and will be reported in due course.

CONCLUSIONS

We present a sensitive and label-free method of detecting *S. aureus* and other bacterial pathogens based on Fourier peak intensities derived from periodic arrays of immutable ligands. Inkjet printing is an excellent method for producing microarrays of ligands mounted on carrier proteins, which can be deposited with spot sizes and lattice spacings in the range of tens of micrometers. The immutable ligand arrays are able to generate bacterial capture patterns with low background noise, which can be imaged with high contrast under simple darkfield conditions and decoded by a FFT-based algorithm to produce readouts with LODs at or below 10^3 cfu/mL. Our FFT-based approach can also produce independent readouts from multiple arrays on the same substrate without compromising signal quality, with further improvements possible by increasing the size of the ROI or refining the array structures. Inkjet printing of protein conjugates into microarrays can be extended to other types of capture ligands, such as siderophores, aptamers, lectins, and antibodies, to support the development of complex patterns consisting of orthogonal ligands for multiplex pathogen detection, with capture specificities encoded by the unique characteristics of each lattice.

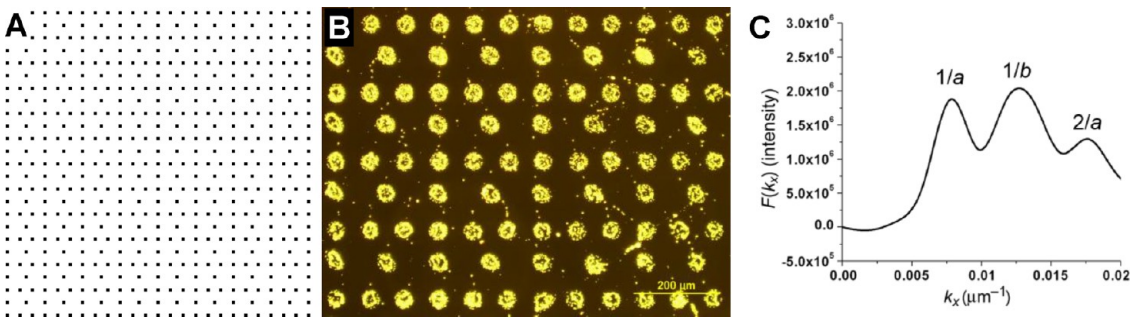

Figure 7. Printing and FFT analysis of interdigitated arrays of **1**-BSA using two different periods. (A) Bitmap image of a centroid map used to print binary arrays in alternating rows. Elements are spaced 4 or 6 pixels apart along the x direction (80 and 120 μm, respectively); rows are spaced 4 pixels apart along the y direction (80 μm). (B) Darkfield image of the binary capture array after 1-h exposure to *P. aeruginosa* (10^6 cfu/mL). (C) FFT analysis of the capture array after image processing, with two well-defined fundamental harmonic peaks ($1/a$ = 1/120 μm^{-1}; $1/b$ = 1/80 μm^{-1}) and a second-order harmonic peak ($2/a$ = 1/60 μm^{-1}).

dx.doi.org/10.1021/am4016236 | ACS Appl. Mater. Interfaces 2013, 5, 6404−6411

■ ASSOCIATED CONTENT

Supporting Information

Mass spectral data of **1**-BSA; schematic and photograph of thermal inkjet deposition system; inkjet printing of **1**-BSA in buffered solution with varying amounts of surfactant; SYTO-9/PI staining of captured bacteria. This material is available free of charge via the Internet at http://pubs.acs.org.

■ AUTHOR INFORMATION

Corresponding Author

*E-mail: alexwei@purdue.edu.

Notes

The authors declare no competing financial interest.

■ ACKNOWLEDGMENTS

The authors gratefully acknowledge financial support from the Department of Defense (W911SR-08-C-0001) administered through the U.S. Army RDECOM (Edgewood Contracting Division), and the Center for Sensing Science and Technology at Purdue University. We thank Youngsoon Kim and Rajesh Pandey for their assistance with bacteria culture and quantitative cell count.

■ REFERENCES

(1) Deisingh, A. K.; Thompson, M. *Analyst* **2002**, *127*, 567−581.
(2) Struelens, M.; Denis, O.; Rodriguez-Villalobos, H. *Microbes Infect.* **2004**, *6*, 1043−1048.
(3) Centers for Disease Control and Prevention. *MMWR Morb. Mortal. Wkly. Rep.* **1992**, *41*, 783−787.
(4) Diekema, D. J.; Boots Miller, B. J.; Vaughn, T. E.; Woolson, R. F.; Yankey, J. W.; Ernst, E. J.; Flach, S. D.; Ward, M. M.; Franciscus, C. L. J.; Pfaller, M. A.; Doebbeling, B. N. *Clin. Infect. Dis.* **2004**, *38*, 78−85.
(5) Deurenberg, R. H.; Vink, C.; Kalenic, S.; Friedrich, A. W.; Bruggeman, C. A.; Stobberingh, E. E. *Clin. Microbiol. Infect.* **2007**, *13*, 222−235.
(6) Deresinski, S. *Clin. Infect. Dis.* **2005**, *40*, 562−573.
(7) Tenover, F. C.; Pearson, M. L. *Emerging Infect. Dis.* **2004**, *10*, 2052−2053.
(8) Schmid-Hempel, P.; Frank, S. A. *PLoS Pathog.* **2007**, *3*, 1372−1373.
(9) Skottrup, P. D.; Nicolaisen, M.; Justesen, A. F. *Biosens. Bioelectron.* **2008**, *24*, 339−348.
(10) Kulkarni, A. A.; Weiss, A. A.; Iyer, S. S. *Med. Res. Rev.* **2010**, *30*, 327−393.
(11) Karlsson, K.-A. *Curr. Opin. Struct. Biol.* **1995**, *5*, 622−635.
(12) Krivan, H. C.; Roberts, D. D.; Ginsburg, V. *Proc. Natl. Acad. Sci. U.S.A.* **1988**, *85*, 6157−6161.
(13) Mason, H. Y.; Lloyd, C.; Dice, M.; Sinclair, R., Jr.; Ellis, W.; Powers, L. *Biosens. Bioelectron.* **2003**, *18*, 521−527.
(14) Adak, A. K.; Leonov, A. P.; Ding, N.; Jyothi, T.; Kularatne, S.; Low, P. S.; Wei, A. *Bioconjugate Chem.* **2010**, *21*, 2065−2075.
(15) Doorneweerd, D. D.; Henne, W. A.; Reifenberger, R. G.; Low, P. S. *Langmuir* **2010**, *26*, 15424−15429.
(16) Kim, Y.; Lyvers, D. P.; Wei, A.; Reifenberger, R.; Low, P. S. *Lab Chip* **2012**, *12*, 971−976.
(17) Ymeti, A.; Kanger, J. S.; Greve, J.; Lambeck, P. V.; Wijn, R.; Heideman, R. G. *Appl. Opt.* **2003**, *42*, 5649−5660.
(18) Massad-Ivanir, N.; Shtenberg, G.; Zeidman, T.; Segal, E. *Adv. Funct. Mater.* **2010**, *20*, 2269−2277.
(19) Massad-Ivanir, N.; Shtenberg, G.; Tzur, A.; Krepker, M. A.; Segal, E. *Anal. Chem.* **2011**, *83*, 3282−3289.
(20) Walz, A.; Odenbreit, S.; Mahdavi, J.; Borén, T.; Ruhl, S. *Glycobiology* **2005**, *15*, 700−708.
(21) Stevens, J.; Blixt, O.; Paulson, J. C.; Wilson, I. A. *Nat. Rev. Microbiol.* **2006**, *4*, 857−864.
(22) Delehanty, J. B.; Ligler, F. S. *Anal. Chem.* **2002**, *74*, 5681−5687.
(23) Horcas, I.; Fernandez, R.; Gomez-Rodriguez, J. M.; Colchero, J.; Gomez-Herrero, J.; Baro, A. M. *Rev. Sci. Instrum.* **2007**, *78*, 013705.
(24) Leonov, A. P.; Wei, A. *J. Mater. Chem.* **2011**, *21*, 4371−4376.
(25) Calvert, P. *Chem. Mater.* **2001**, *13*, 3299−3305.
(26) Tekin, E.; Smith, P. J.; Schubert, U. S. *Soft Matter* **2008**, *4*, 703−713.
(27) de Gans, B. J.; Duineveld, P. C.; Schubert, U. S. *Adv. Mater.* **2004**, *16*, 203−213.
(28) Schena, M.; Heller, R. A.; Theriault, T. P.; Konrad, K.; Lachenmeier, E.; Davis, R. W. *Trends Biotechnol.* **1998**, *16*, 301−306.
(29) Okamoto, T.; Suzuki, T.; Yamamoto, N. *Nat. Biotechnol.* **2000**, *18*, 438−441.
(30) Weissenstein, U.; Schneider, M. J.; Pawlak, M.; Cicenas, J.; Eppenberger-Castori, S.; Oroszlan, P.; Ehret, S.; Geurts-Moespot, A.; Sweep, F. C. G. J.; Eppenberger, U. *Proteomics* **2006**, *6*, 1427−1436.
(31) Delaney, J. T.; Smith, P. J.; Schubert, U. S. *Soft Matter* **2009**, *5*, 4866−4877.
(32) Roth, E. A.; Xu, T.; Das, M.; Gregory, C.; Hickman, J. J.; Boland, T. *Biomaterials* **2004**, *25*, 3707−3715.
(33) Thomas, R.; Brooks, T. *J. Med. Microbiol.* **2004**, *53*, 833−840.
(34) Hansen, F. K.; Rødsrud, G. *J. Colloid Interface Sci.* **1991**, *141*, 1−9.
(35) Iqbal, S. S.; Mayo, M. W.; Bruno, J. G.; Bronk, B. V.; Batt, C. A.; Chambers, J. P. *Biosens. Bioelectron.* **2000**, *15*, 549−578.
(36) Boujday, S.; Briandet, R.; Salmain, M. l.; Herry, J.-M.; Marnet, P.-G.; Gautier, M.; Pradier, C.-M. *Microchim. Acta* **2008**, *163*, 203−209.
(37) Subramanian, A.; Irudayaraj, J.; Ryan, T. *Sens. Actuators B* **2006**, *114*, 192−198.
(38) Thomas, R.; Brooks, T. *J. Med. Microbiol.* **2006**, *55*, 309−315.